Chemichal and Thermal Changes in $Mg_3Si_2O_5(OH)_4$ Polimorf Minerals and Importance as a Industrial Material

Ahmet Sasmaz *, Ayşe Didem KILIÇ *, Nevin Konakcı *

Posted Date: 25 September 2024

doi: 10.20944/preprints202409.1957.v1

Keywords: geological materials; DTA; TG; hydrothermal alteration; ophiolite

Article

Chemichal and Thermal Changes in $Mg_3Si_2O_5(OH)_4$ Polimorf Minerals and Importance as a Industrial Material

Ahmet ŞAŞMAZ, Ayşe Didem KILIÇ * and Nevin KONAKCI

Department of Geological Engineering, Fırat University, 23119 Elazığ, TÜRKİYE
* Correspondence: adkilic@firat.edu.tr

Abstract: Serpentine ($Mg_3Si_2O_5(OH)_4$), like quartz, dolomite and magnesite minerals, is a versatile mineral group characterized by silica and magnesium silicate contents with multiple polymorphic phases. Among the phases composed of antigorite, lizardite, and chrysotile, lizardite and chrysotile are the most prevalent phases in the serpentinites studied here. The ΣLREE/ΣHREE ratios of the samples are between 0.16 and 4 ppm. While Ce shows a strong negative anomaly (0.1–12), Eu shows a weak positive anomaly (0.1–0.3). This indicates that fluid interacts significantly with rock during serpentinization, and Highly Incompatible Elements (HIEs) gradually become involved in the serpentinization process. The large differential thermal analysis (DTA) peak at 810–830 °C is an important sign of dehydration, transformation reactions and thermal decomposition, and is com-patible with H_2O phyllosilicates in the mineral structure losing water at this temperature. In SEM images, chrysotile, which has a fibrous structure, and lizardite, which has a flat appearance, trans-form into talc as a result of dehydration with increasing temperature. Therefore, the sudden tem-perature drop observed in DTA graphs is an indicator of crystal form transformation and CO_2 loss. In this study, the mineralogical and structural properties and the formation of serpentinites were examined for the first time using thermo-gravimetric analysis methods. In addition, the mineralogical and physical properties of serpentinites can be recommended for industrial use as additives in polymers or in the adsorption of organic pollutants. As a result, the high refractory nature of examined serpentine suggests that it is well-suited for applications involving high temperatures. This includes industries such as metallurgy and steel production, glass manufacturing, ceramic production, and the chemical industry.

Keywords: geological materials; DTA; TG; hydrothermal alteration; ophiolite

1. Introduction

Anatolia, located in the Alpine orogenic belt on the southern branch of the Neotethys, consists of ultramafic rocks spread over wide areas (Figure 1). The study area (Alacaka-ya-Elazığ) on the Eastern Anatolian fault zone bears traces of serpentinization, carbona-tion, ophicalsite formations and lisvenitization, developed under the influence of tec-tonism. The ocean, which was formed in the Middle-Upper Triassic by the rifting of the Cimmerian Continent surrounding Turkey, was most extensive in the Jurassic-Lower Cre-taceous. In the Upper Cretaceous, the southern branch of the Neotethys disappeared by diverting towards the north. The ophiolites, which were first settled towards the end of the Cretaceous, continued to settle towards the south with Eocene–Miocene compressional tectonics [1,2].

Serpentinite is a metamorphic rock composed mostly of serpentine group minerals such as lizardite, antigorite and chrysotile. This rock, which has fascinating shades of green, is usually banded or layered. Serpentine is a mineral group consisting of about twenty minerals with a general chemical composition typically represented as Mg3-(M), Si2-(T) and O5(OH)4, where the M site can be filled by Fe3+, Mg2+, Fe2+, Mn2+, Al3+, Zn2+ or Ni2+ and the T site by Si4+, Fe3+, or Al3+. These minerals are formed through the hydration of oli-vine-(Mg2+, Fe2+)2 SiO4 in silica-poor serpentinites at relatively low temperatures [3]. The serpentine group contains three main minerals of antigorite,

 doi:10.20944/preprints202409.1957.v

chrysotile or lizarrite [4]. The formation of antigorite, lizardite and chrysotile minerals by the crystallization of structur-ally different serpentine B polymorphs constitutes the serpentinization process [5–7]. Low-grade serpentinites include lizardite and chrysotile [8]. Current studies [6,8] show that serpentinization occurs due to the hydration effect in the initial phase, with an ap-proximately 20-40% volume increase. There is no significant dissolution, except for of H2 (McCollom and Bach 2009). The increase in volume creates a fracture system. The serpen-tine minerals, especially fibrous B polyform (chrysotile), break as the serpentinite does not expand to cover the increase in volume [9,10].

Based on thermodynamic data, Evans [6] reported that, above 300 °C, the an-tigorite+brucite assemblage is more stable than lizardite, and chrysotile is absent. The an-tigorite + brucite assemblage is frequently observed in serpentinites, while chrysotile + brucite is more abundant in serpentinites that have undergone regressive metamorphism [8]. Johannes [11] indicated serpentinization temperatures of 350–425 °C for chrysotile, 500 °C for antigorite (according to Barnes and O'Neil [10]) and 440 °C for lizard-ite+chrysotile (according to Moody) [12].

Serpentinization is a process characterized by reduction–oxidation and dissolution–precipitation reactions when ultramafic rocks are exposed to water and fractured at the crustal level. When primary silicates transform into serpentines, the density varies be-tween 3.3 and 2.7 g/cm3, and there is a significant increase in volume. The clearest result of this is seen in the fracture system, in which newly formed serpentine minerals, especially the fibrous B polyform, are formed. This fracture represents an attempt to accommodate the volume increase of the non-expandable serpentinite [18,19]. Evans et al. [7] indicated a di-rect connection between serpentinization and arc magmatism. Previous studies have stat-ed that ocean floor spreading is the only pathway for the hydrothermal alteration of ser-pentinites in ultramafic rocks in the mantle. The combination of magnetite and antigorite is only possible in ocean floor serpentinization. This serpentinization produces serpentine minerals, Fe–Ni alloys, magnetite, alkaline solutions and gases (H2, CH4) [13–15]. During serpentinization, water is consumed, but no significant dissolved components other than H2 are released [16,17]. The hydration of mantle peridotite with seawater causes the oxi-dation of Fe in primary minerals (pyroxene and olivine) to Fe (III) in secondary phases, following the reaction 2 FeO + H2O = Fe2O3 + H2 [18]. The main hosts of ferric Fe are magnetite, Fe3+2Fe2+O4 and Fe3+-serpentine minerals. Magnetite is very rarely seen in mantle wedge serpentinization. Mantle wedge serpentinites rarely contain magnetite. This is due to the high-T regime, characterized by the rapid diffusion rates of Fe–Mg above 400 °C, and thermodynamic equilibrium can only be reached above 600 °C [19]. Ulmer and Trommsdorff [20] stated that serpentine minerals, with a total weight of ~13% H2O, are important in the water cycle in subduction zones and in the melting of heat flow in the mantle wedge.

Serpentinite can be used in different areas (construction, ceramics, agriculture, min-ing, steel, etc.) due to its physical properties, especially the presence of high Mg and Si concentrations, as well as its surface properties [21]. The serpentinite group is a potential source due to the high magnesium content of the protolith. Today, the use of serpentinites in agriculture is being investigated in countries with temperate climates. Some studies have been conducted to evaluate serpentinite minerals' performance as agricultural and magnesium fertilizers. For example, a study conducted in New Zealand evaluated the performance of serpentinites and dunites as magnesium sources [22]. Another study ex-amined the effects of serpentinite magnesium fertilizer on feed efficiency [23] and Błońska et al. [24] examined the effect of serpentinite soil on nutrients in Poland. Luz et al. [25] evaluated the agricultural potential of serpentinites in Brazil, and Carmignano [26] the performance of serpentinites in soybean crops.Blaskowski et al. [27] the agricultural po-tential of mining wastes consisting of dunite and serpentinite. Lizardite from serpantinite minerals used as an additive in ceramic and glass production. It especially plays a role in the production of ceramics resistant to high temperatures. It can be used in construction materials, especially stone blocks and paving materials [28]. Chrysotile has been widely used in thermal insulation and fire protection applications. As regards the mechanical and industrial applications, chrysotile has been used in a variety of industrial applica-tions, especially where heat and wear resistance is required. Chrysotile is frequently used as

 doi:10.20944/preprints202409.1957.v

a firefighting material [29]. It is used in the automotive industry, in brake pads and clutch systems [30], and as an insulation material in electrical devices to provide heat and wear resistance [31]. One of the countries that uses chrysotile the most to produce friction materials is Iran (2000 tons every year) [32]. Chrysotile is used as a filler for asphalt pave-ment and resin plastics on traffic roads. In industrial applications, chrysotile is used by combining it with phenolic polypropylene and plastics in heating systems and industrial furnaces, coatings, packaging materials, aircraft wing fuel tanks, rocket tail nozzle tubes, rocket ablation prevention materials. Among the many industrial applications of chryso-tile, 80% for construction materials, asbestos sheet and cement products, 7% for friction materials; and a usage of <3% has been reported for chrysotile textiles [33]. In building materials, chrysotile can be used as ceiling flooring, roof tiles, sound insulation boards, house panels, pipe insulation and wall panels. Additionally, various chrysotile cement products are also used today [34]. Similarly, it is used to produce vitrified materials and for cathode ray tube (CRT) glass parts [35]. In terms of environmental benefits and safety, alternative asbestos materials are among the most researched topics today to avoid the use of chrysotile [36].

Serpentinites are distributed across various regions worldwide, with global reserves estimated to be in the hundreds of millions of tons. Serpentinite reserves can be found in Australia, Paraguay, Italy, New Zealand, Russia, Canada, the USA, Brazil and Türkiye [37,38]. There are serpentinite and serpantinize ultramaphites within the Guleman, Koçali and Kömürhan ophiolites on the Eastern Anatolian Fault zone (Figure 1).

This study, aimed to determine the petrographic and geochemical properties, geotec-tonic environments of the Guleman ophiolite serpantinites, as well as to determine the ag-ricultural and industrial importance of serpentine minerals.

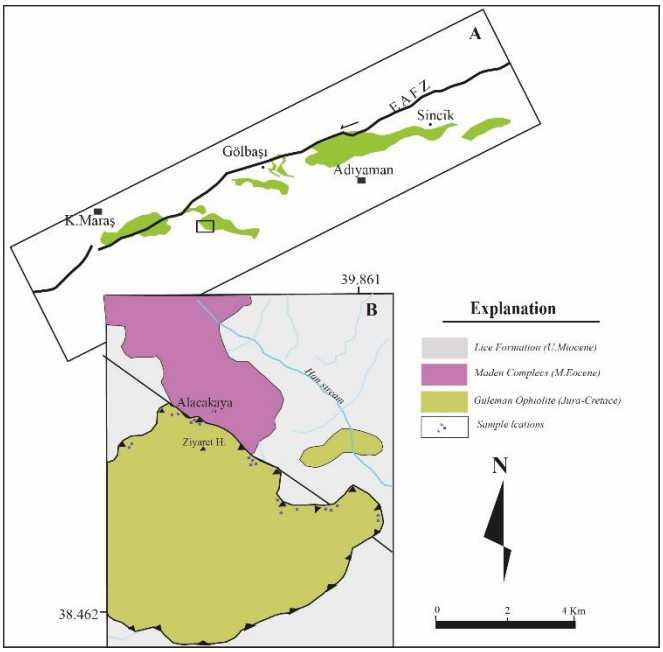

Figure 1. A) Regional geological map of the study area [2]. B) Simplified geological map [1].

2. Materials and Methods

Serpentinite, which has industrial importance, was examined as a novel material. The ICP-MS NexION 2000 (Perkin Elmer Inc., USA) device, which includes a quartz nebulizer gasifier, cyclonic spray circle and an integrated auto-sampler, was used for oxide and ele-mental analyses of the samples. Using 18.3 MΩ ultrapure water obtained from the Human Power I device, a solution containing 1% hydrochloric acid–ultrapure water was weighed and mixed with approximately 0.5 grams of the samples during sample preparation. Cem brand Mars 6 One Touch (USA) was transferred to Teflon microwave containers and pre-pared in the microwave by adding 10 mL of concentrated nitric acid to each sample. ICP-MS calibration solutions were prepared by diluting commercially available mul-ti-element standards with 1% (nitric acid–ultra pure water) at the

 doi:10.20944/preprints202409.1957.v

concentrations specified in Table 1. Additionally, ICP-MS calibration was performed before each measurement. For the control of elemental analyses, 100 ppb 45Sc, 89Y, 209Bi was used as the internal standard. The results obtained are listed in Table 1.

 doi:10.20944/preprints202409.1957.v1

Table 1. Results of major oxide and some trace elemental analyses of serpentinite by LA-ICPMS.

Major Oxides	Na_2O	MgO	Al_2O_3	SiO_2	P_2O_5	K_2O	CaO	TiO_2	MnO	Fe_2O_3	LOI	TOTAL	Sc	V	Co	Ni	Cu	Zn	Ga	Rb	Sr	Y	Zr	Nb	Mo	Cd
Sp-01	0.3	22.8	6.9	37.3	0.1	1.1	4.5	0.2	0.3	5	11.3	99.6	20	72	18	1001	14	35	9.9	10	102	7.3	19	2.4	5	0.1
Sp -03	0.1	38.8	0.5	40.4	0.1	0.1	0.1	0.1	0.1	7.4	11.8	100.4	4	12	87	965	3	26	0.9	10	10	0.2	2	0.1	5	2
Sp -04	0.1	34.9	0.6	35.1	0.1	0.1	4.9	0.1	0.1	7.2	11.4	100.4	3	12	91	972	19	446	1.1	10	32	0.4	2.9	0.2	5	2
Sp -06	0.1	38.2	0.3	41.9	0.1	0.1	0.2	0.2	0.1	6.6	11.6	100.6	6	16	75	1545	3	42	1.7	10	10	0.1	1.6	0.1	5	0.6
Sp -08	0.1	37.7	0.8	41.5	0.1	0.1	0.1	0.1	0.1	6.6	11.3	100.2	8	27	73	1819	4	26	2	10	10	0.2	1.9	0.1	5	1.1
Sp -09	0.1	37.2	0.8	42.1	0.1	0.1	0.4	0.1	0.2	6.6	9.1	100.1	5	15	54	1197	4	32	2.2	10	10	14.4	2.6	1	5	0.8
Sp -10	0.1	37.3	2.6	38.3	0.1	0.1	0.1	0.1	0.3	9	8.0	99.9	9	24	81	727	5	35	1.1	10	10	1.5	2.7	0.1	5	1.6
Sp -11	0.1	33.5	1.9	37.8	0.1	0.1	4.23	0.1	0.1	8.3	1.6	99.8	7	33	96	1184	15	34	1	10	29	1.2	3.4	0.1	5	1.1
Sp -12	0.1	36.7	0.5	37.1	0.1	0.1	2.6	0.1	0.1	6.7	3.4	99.8	20	44	82	1757	24	44	0.8	10	140	0.4	2.5	0.1	5	0.8
Sp -14	0.1	38.5	0.6	39.3	0.1	0.1	1	0.1	0.1	74	1.3	99.9	6	36	74	1503	17	33	1.1	10	20	0.3	2	0.1	5	1.1
Sp -15	0.1	38.4	0.8	41.8	0.1	0.1	0.2	0.1	0.1	10	1.3	99.9	7	19	96	2033	19	34	0.8	10	10	0.4	2.3	0.1	5	1.1
Sp -16	0.1	37.6	0.8	40	0.1	0.1	0.1	0.1	0.1	7.9	1.9	99.9	5	31	74	1513	12	31	1.5	10	10	0.3	1.9	0.1	5	1.3
Sp -17	0.1	37.9	0.6	40.1	0.1	0.1	0.8	0.1	0.1	10.6	1.4	99.9	12	28	75	1739	13	29	0.7	10	10	0.1	1.9	0.1	5	0.7
Sp -18	0.1	36.2	0.8	38.4	0.1	0.1	2.4	0.1	0.1	7.9	1.2	99.8	8	43	89	1019	113	47	0.9	10	10	2.8	2.6	0.1	5	1.5
Sp -21	0.1	38.1	0.4	37.7	0.1	0.1	0.5	0.1	0.2	10.0	1.7	99.9	9	26	80	1740	7	41	0.7	10	10	0.2	1.3	0.1	5	0.7
Sp -23	0.1	41.1	0.7	43.1	0.1	0.1	0.8	0.1	0.1	9.67	1.7	99.9	0	15	73	1687	11	36	0.9	10	10	0.1	1.6	0.1	5	1.1
Sp -24	0.1	42.1	0.6	41.7	0.1	0.1	3.42	0.1	0.1	7.1	1.4	99.8	0	27	91	1860	23	41	0.9	10	10	0.6	1.5	0.1	5	0.9
Sp -25	0.1	36.7	3.3	37.4	0.1	0.1	5.1	0.1	0.1	7.8	2.0	99.8	0	37	79	1175	4	28	2.9	10	75.4	2.7	4.5	0.3	5	0.8
Sp -27	0.1	33.8	3.3	40.0	0.1	0.1	1	0.1	0.1	9.1	1.4	99.8	0	34	68	1323	20	37	2.1	18	10	2.8	4.6	0.3	5	0.7

 doi:10.20944/preprints202409.1957.v

(Continuied Table 1).

Trace Elements	Ba	Ti	Cr	Sn	Mn	Cs	Ta
Sp-01	33	22	226	10	814	1,1	0,2
Sp -03	49	32	233	11	803	0,1	0,1
Sp -04	<10	32	432	10	619	0,1	<0.1
Sp -06	<10	36	625	10	934	1,2	<0.1
Sp -08	<10	32	112	11	722	0,1	<0.1
Sp -09	<10	30	201	<10	274	0,1	<0.1
Sp -10	<10	66	772	<10	565	0,1	<0.1
Sp -11	<10	33	381	<10	415	0,1	<0.1
Sp -12	<10	34	206	<10	324	0,1	<0.1
Sp -14	<10	55	189	<10	217	0,1	0,1
Sp -15	<10	58	204	<10	219	0,1	0,1
Sp -16	<10	37	311	<10	812	0,1	<0.1
Sp -17	<10	44	197	<10	613	0,1	0,1
Sp -18	<10	31	312	<10	913	0,1	<0.1
Sp -21	<10	52	423	<10	577	0,1	<0.1
Sp -23	<10	35	178	<10	311	0,1	<0.1
Sp -24	<10	37	120	10	293	0,1	<0.1
Sp -25	<10	33	344	<10	435	0,1	<0.1
Sp -27	<10	34	221	<10	209	0,1	<0.1

DTA/TG, SEM and XRD analyses of the selected samples were performed in Erzincan Binali Yıldırım University Physics laboratory. DTA/TG analyses were kept at 900 °C for 10 minutes in a Hitachi brand device. Serpentine samples were ground until they reached a homogeneous size (usually 10-20 mg). The sample was placed into a DTA sample holder. The powdered sample was compressed into a container made of an inert material (plati-num). In DTA/TG analyses, alumina powder is generally used as an inert reference mate-rial. The heating rate is set (usually 10-20 °C per minute) and the maximum temperature is adjusted to 900 °C. The device is started, and the response of the sample to the increasing temperature is observed. DTA records the temperature differences between the reference and the sample. Endothermic or exothermic events (e.g., phase transitions, decomposition reactions) related to the temperature change are monitored and plotted on a graph. Sample graphs and temperature changes are shown in Figure 6.

High-resolution scanning electron microscopy was used to analyze the microstruc-tural properties of the samples. Electron microscope images were taken directly from the external surfaces of the samples. Samples were prepared for SEM analyses. Fresh samples for SEM analysis. The other 5 faces were turned into smooth surfaces so that the broken surface was protected. This process was carried out at Erzincan Binali Yıldırım University Faculty of Science Center. It was made in his laboratory. These samples were then coated with gold under vacuum in the SEM laboratory of EBYU Department of Physics. SEM analyses were performed using a QUANTA FEG 450 model electron microscope. Granular structures could be clearly observed in the SEM photographs. SEM microphotographs taken at different magnifications of samples partially doped with Ag instead of Bi are shown in Figure 3. Fibrous, plate- or needle-like structures can be seen in the serpentinites [15].

X-ray diffraction patterns were examined to determine the serpentine types. Using these patterns, information about the crystal structures could be obtained regarding the lattice parameters and Miller indices of the material. It is also necessary to obtain the X-ray powder diffraction pattern to detect different phases and impurity phases in the sample. For this purpose, we pulverized the sintered materials in an agate mortar and prepared them for XRD analysis. These analyses were carried out in the range of $5^o \leq 2\theta \leq 60^o$ using CuKα X-rays on QUANTA FEG-450 Powder. XRD patterns of the samples are shown in Figure 8.

 doi:10.20944/preprints202409.1957.v

3. Results

The serpentinites found in ultramaphites belonging to the Guleman ophiolite in the study area, comprising the Elazığ-Alacakaya district on the Alpine orogenic belt, were massive, and exhibited the mesh and bastite textures typical of hydrated oceanic perido-tites [3,22], intersected by multiple generations of serpentine veins (Figure 2). In the samples, they were revealed to be predominantly grayish to dark greenish, medium- to coarse-grained, and characterized by interlocking textures (Figure2B,D). Many samples dis-played crude foliation with shear planes, along with lineation marks (slickensides) and remnants of serpentine patches on their surfaces.

In the samples examined, serpentinization was almost complete, and primary mineral inclusions (pyroxene, olivine, spinel) were rarely observed. Olivine and/or pyroxene were accompanied by iron oxides distributed heterogeneously within the network fabric. Spinels were frequently oxidized (Figure 3). The partial preservation of the original mesh texture of the main minerals (olivine and orthopyroxene) shows that the temperature was not very high, and the serpentinized parent rock had a high mafic mineral content (Figure 2A,B). The orthopyroxene was replaced with chrysotile, forming a network around the rel-ic minerals [7,13,21,26] (Figure 3). The hydration of the orthopyroxe mineral was pseudo-morphic. The serpentine, which was determined to have a reticular texture, and lizardite were the products of the serpentinization of orthopyroxene, since the rock was chrysotile and predominantly lizardite (SiO_2 < %44 at lizardite–chyrysotile). The SiO_2 content of the samples was <44%, and the SEM images show chrysotile+lyzarite. The combination of these two minerals indicates a temperature of approximately 400 °C. Also, morphological-ly speaking, serpentinites exhibit a platy or flaky habit, are often fibrous, have a soapy texture, and are predominantly composed of chrysotile and lizardite. Dehydration during formation at high temperatures can lead to talc formation. The typical pseudomorphs may change as the processes of metamorphism and shearing progress. Lizardite is occasionally found in elongated patches aligned parallel to the slip direction along the foliation (Figure 3), while chrysotile has a typical fibrous appearance (Figure 2).

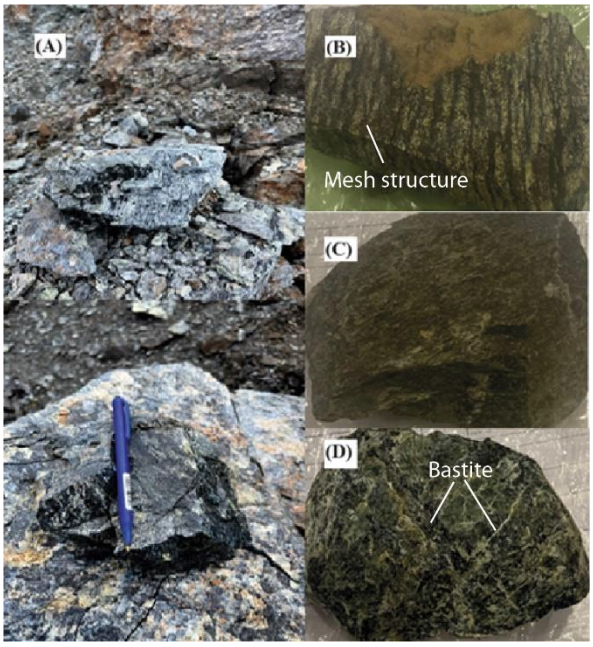

Figure 2. Serpentinite samples with mesh (A,B) and bastite (C,D).

 doi:10.20944/preprints202409.1957.v

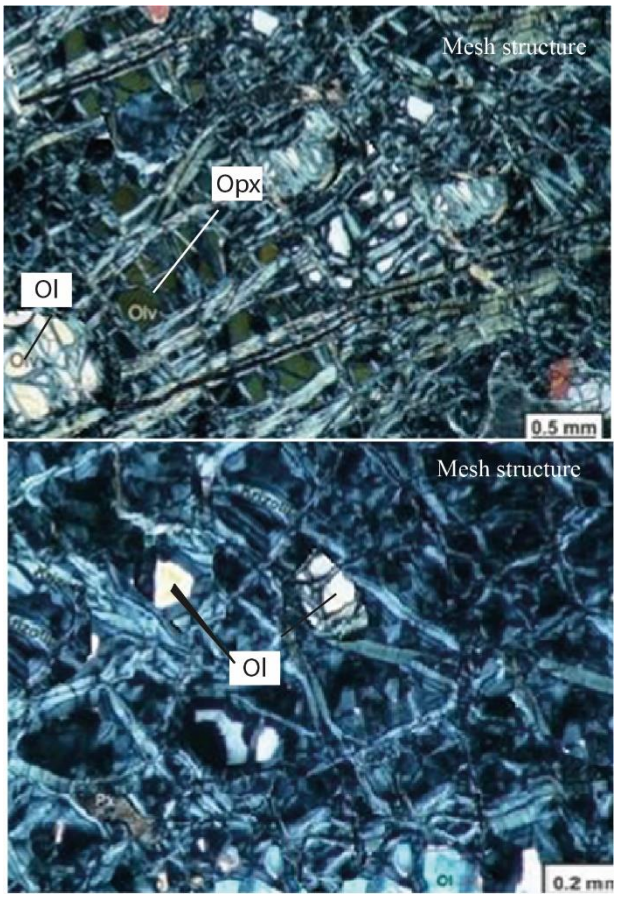

Figure 3. The features of microstructure of serpentinite. Residual minerals surrounded by lizardite and chrysotile.

3.1. Geochemistry

The bulk chemical composition of the investigated serpentinites featured low contents of SiO2 (39.52% on average) and TiO2 (0.1–0.2% by weight), high MgO (36.67% average) and Na2O (0.1% on average) contents, and Al2O3 contents that were moderate to high (0.3 to 16.9 wt. %) (Table 1). The CaO content was high, at 1.70% on average. The substitution of Mg with Fe in antigorite, in contrast with the exclusive presence of Mg in pure lizardite, underscores the findings that lizardite is more conducive to carbonation compared to an-tigorite [10,28]. The total Fe2O3 content was also high (5–10.6 wt. %) (Table 1). The Mg/Si ratio of serpentinite samples was between 1.18 and 1.38 (~1.33) and Mg# [Mg/(Mg+Fe)] 0.78–0.92, indicating that mantle peridotites in MOR (Mg# 0 .89–0.92) feature a different formation environment, or that the environment has changed in subsequent processes. The total Ni content of the samples is 1001–2033 ppm.

The analysis results are listed in Tables 1 and 2. The ΣREE values of serpentin-ites varied between 2.51 and 3.42 ppm. While the ΣLREE contents ranged from 1.58 to 2.67 ppm, the ΣHREE contents ranged from 0.87 to 0.96 (Figure 3a,b) (Table 2). The ΣLREE/ΣHREE ratios were between 1 and 3, with Ce showing a strong negative anomaly (0.1–12) and Eu shooing a weak positive anomaly (0.1–0.3) (Figure 4b). The presence of these elements indicates rock–water interaction during serpentinization, and the evidence of the gradual release of Highly Incompatible Elements (HIEs) indicates functions resulting from fluid integration into the system and following a subduction process [23]. Furthermore, the positive Eu anomaly can also be attributed to the formation of lizardite during ocean ser-pentinization or the dissolution of plagioclase in hydrothermal fluid circulation [25,26]. This suggests that oceanic serpentinization fluid leaches Eu during fluid–rock interaction, rather than reacting with the plagioclase of the serpentinites [29-31. The enrichment in LREE and HREE ratios occurs after melting or during melting due to the interactions with liquid [29]. The

 doi:10.20944/preprints202409.1957.v

moderate siderophiles Ni and Co [30]; highly siderophile elements Pd, Pt, Cs and Zr [31]; and elements such as F, As, Cl and Sb are found in serpentinites, which shows fluid interaction between the subducted crust and sediments during the hydration of peridotites [32–34].

 doi:10.20944/preprints202409.1957.v1

Table 2. Rare earth element analysis results of serpentinites.

	La	Ce	Pr	Nd	Sm	Eu	Gd	Tb	Dy	Ho	Er	Tm	Yb	Lu	∑REE	∑LREE	∑HREE
Sp-01	0.90	0.48	0.16	0.34	0.22	0.11	0.18	0.18	0.18	0.08	0.19	0.05	0.18	0.04	3.29	2.39	0.90
Sp -03	0.35	0.27	0.12	0.38	0.18	0.12	0.22	0.22	0.16	0.09	0.18	0.04	0.17	0.05	2.55	1.64	0.91
Sp -04	0.44	0.42	0.10	0.36	0.21	0.11	0.20	0.18	0.19	0.10	0.18	0.04	0.17	0.04	2.74	1.84	0.90
Sp -06	0.88	0.32	0.11	0.37	0.15	0.13	0.19	0.21	0.17	0.09	0.20	0.05	0.19	0.04	3.10	2.15	0.95
Sp -08	0.66	0.44	0.13	0.42	0.16	0.12	0.24	0.16	0.18	0.08	0.19	0.04	0.18	0.05	3.05	2.17	0.88
Sp -09	0.92	0.42	0.18	0.38	0.22	0.13	0.23	0.19	0.19	0.07	0.21	0.04	0.20	0.04	3.42	2.67	0.94
Sp -10	0.38	0.30	0.12	0.36	0.18	0.10	0.26	0.17	0.19	0.08	0.22	0.05	0.21	0.05	2.67	1.70	0.97
Sp -11	0.23	0.31	0.12	0.44	0.21	0.12	0.18	0.18	0.16	0.08	0.22	0.04	0.18	0.04	2.51	1.61	0.90
Sp -12	0.44	0.40	0.10	0.35	0.15	0.13	0.22	0.16	0.16	0.09	0.18	0.05	0.19	0.04	2.66	1.79	0.87
Sp -14	0.36	0.29	0.09	0.34	0.16	0.14	0.21	0.20	0.18	0.08	0.19	0.04	0.20	0.05	2.53	1.59	0.94
Sp -15	0.28	0.30	0.11	0.45	0.22	0.13	0.23	0.18	0.16	0.09	0.18	0.05	0.16	0.05	2.59	1.72	0.87
Sp -16	0.36	0.31	0.11	0.42	0.18	0.12	0.24	0.22	0.19	0.09	0.18	0.04	0.19	0.04	2.69	1.74	0.95
Sp -17	0.34	0.33	0.14	0.43	0.21	0.12	0.25	0.16	0.21	0.09	0.20	0.05	0.20	0.05	2.78	1.82	0.96
Sp -18	0.25	0.28	0.10	0.44	0.15	0.14	0.22	0.17	0.18	0.09	0.22	0.05	0.19	0.05	2.53	1.58	0.95
Sp -21	0.22	0.30	0.09	0.46	0.22	0.11	0.18	0.20	0.19	0.08	0.18	0.04	0.21	0.04	2.52	1.58	0.94
Sp -23	0.35	0.30	0.14	0.38	0.18	0.13	0.22	0.18	0.19	0.08	0.22	0.05	0.19	0.05	2.66	1.70	0.96
Sp -24	0.24	0.34	0.13	0.36	0.21	0.12	0.23	0.19	0.17	0.10	0.19	0.04	0.16	0.05	2.53	1.63	0.90
Sp -25	0.33	0.32	0.18	0.43	0.15	0.11	0.24	0.21	0.18	0.09	0.21	0.05	0.20	0.04	2.74	1.76	0.98
Sp -27	0.37	0.28	0.11	0.41	0.16	0.12	0.20	0.18	0.19	0.08	0.20	0.05	0.18	0.05	2.58	1.65	0.93

 doi:10.20944/preprints202409.1957.v

The analyzed samples were serpentines derived from harzburgite (olivin and orthopyroxene in thin sections). The REE compositions of these samples show a compatible distribution (Figure 4a). The REE values of the samples were above ~0.1. While Nd, Ce and Tb showed negative anomalies, the Pr, Eu, Tm and La contents showed positive anomalies in the chondrite diagram. Finally, the serpentinites were depleted or enriched in LREE (from ~0.1 to 100 CI-Chondrite) and had HREE contents varying from 0.1 to ~10 CI-Chondrite. The REE distributions of these serpentinites, which are rich in trace elements (U, K, Cs, Rb), are compatible with the characteristics of subduction zone serpentinites (~100 PM; Figure 3). In addition, serpentinites can be divided into abyssal, mantle wedge and subduction zone according to their formation environments. The amount of Ti is an important indicator for determining the protoliths of serpentinites. Another feature of subduction-zone serpentinites is high Ti (30-500 ppm), Yb (0.02-1 ppm) and Mg (> 0.4 ppm) values [35]. These features are compatible with the analyzed Elazığ serpentinites (Ti 30-66 ppm, Yb 0.1-0.3 ppm, Mg 0.70-0.83 ppm) (Tablo 1).

LREE enrichment indicates that the serpentinites did not undergo partial melting but were formed by melt/rock interaction, and/or were enriched in the subduction zone by fluids during hydration [34,36]. At the same time, these serpentinites were rich in Pb. The fact that this feature, described by Niu [37] in mantle wedge serpentinites and Tonga fore-arc peridotites, is also observed in subduction serpentinites shows that it originates from depleted basaltic magma, as well as abyssal and mantle wedge peridotites. Rock interactions led to a strong enrichment in U. Most of our examples indicated similar behaviors. In geology, chromatographic processes generally concern the separation and analysis of minerals and elements. This process, which is a laboratory technique, is used in the analysis of geological samples. It is important for the separation and analysis of minerals and elements, and the detection of contamination. The percolation of silicate melts through mantle peridotite, whether by reactive porous flow or the chromatographic process (fractionation), results in the enrichment of light rare earth elements (LREE), as well as incompatible elements such as Th and U [38]. Considering the incompatible elements, it can be said that the melt/rock interaction occurring before serpentinization affects the geochemical composition of serpentinites. Trace element enrichments probably originate from the passive continental margin [34]. This is because, at both passive margins, there are high incompatible trace element concentrations due to fluid remixing and smaller partial melting via metasomatizing melts before serpentinization [35,39]. The MgO-SiO_2, MgO-Fe_2O_3 and Ni-Ce diagrams show that the serpentinites examined are lizardite and chrysotile, and that these minerals are accompanied by talc (Figure 4). The serpentinites showed a mineral assemblage of olivine, chrysotil, lizardite, magnetite, brucite, chlorite, talc and carbonate. In the primitive mantle-normalized trace element variation diagrams for fore-arc and MOR serpentinites, enrichments in U, Sb, Rb, Pb, Sr and Li, compared to elements with similar compatibility, characterize subduction zone serpentinites (Figure 3). Strong enrichments in large ion lithophile elements (LILE), especially Cs and Rb (Figure 3), are also similar to what is found in fore-arc serpentinites. At the same time, trace element patterns normalized to the flat primitive mantle with positive U, Rb, Sm and Ti anomalies indicate the interference of fluids in the subduction zone and fore-arc region (Figure 3b). Also, some MOR serpentinites show a positive Eu anomaly Eu_N /Eu_N* (0·65^5·9). However, most of the incompatible trace elements (Nb, Th and Ce) are present in extremely low amounts [36]. The compositional values of serpentinites depend on their characteristics, as shown in the literature [40] (Figure 5)

 doi:10.20944/preprints202409.1957.v

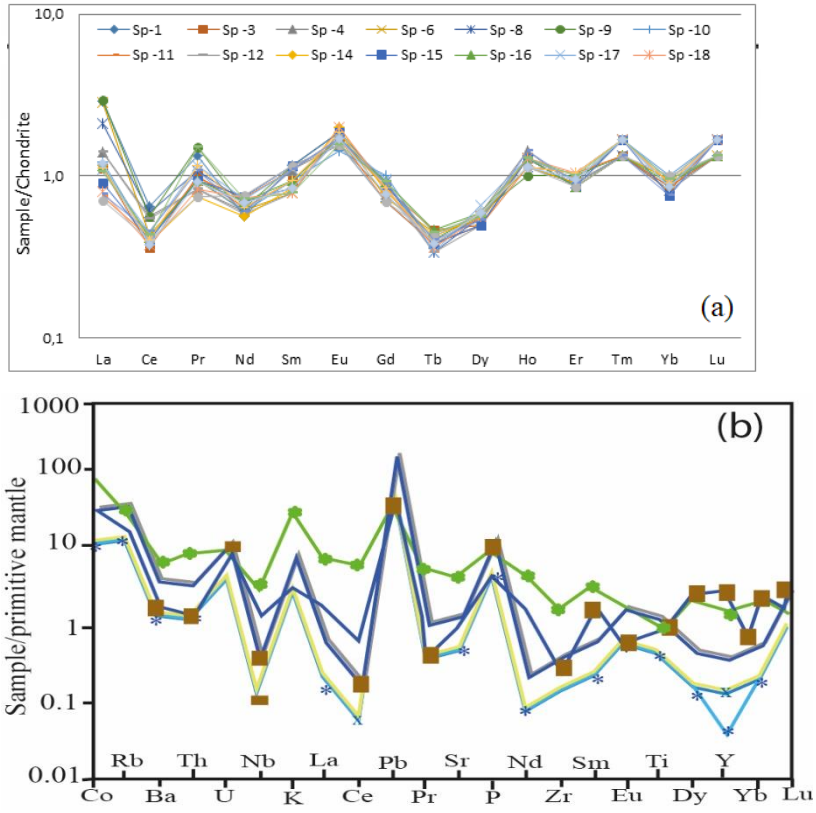

Figure 4. Chondrite (a) and primitive mantle spider (b) diagrams of serpentinites [41].

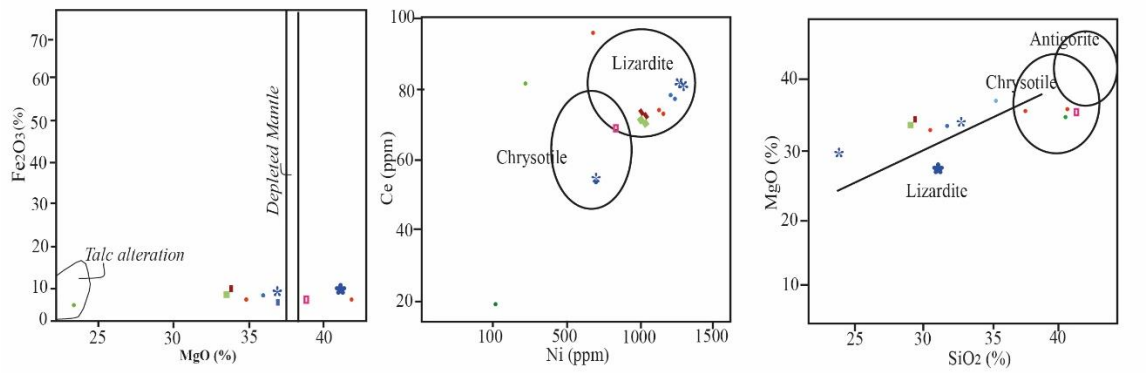

Figure 5. Discriminating diagrams of serpentine minerals [42].

3.2. Thermophysical Properties (SEM, TG, DTA)

The SEM images of samples show chemical color contrasts between dark and very compatibly colored schist serpentine minerals and light gray serpentinite clasts. The SEM examinations show the morphology and changes of serpentine crystals with very small crystal sizes, depicted in Figure 6a-c. As shown in Figure 7a, chrysotile consists of thin and flexible fibrils with a length/diameter ratio of >3 [37], and lizardite has a plate-like morphology, as shown in Figure 7c.

The thermal decomposition of brucite, first with the release of physical water, causes a continuous mass loss until around 500–550 °C [38–40], then the dehydroxylation of layered silicates and the disruption of the crystal lattice occur [42–44]. Another significant thermogravimetric analysis (TGA) confirmed mass loss. The endothermic peak in the differential thermal analysis (DTA) curve and the major exothermic derivative (DTG) peak occurred between 610 and700 °C. Sharp and highly exothermic DTA peaks at approximately 810–830 °C indicate the formation of new minerals such as olivine, pyroxene forsterite or enstatite [40–42]. In the case of sample 6, similar TGA steps are seen, except that the second step is divided into two steps, with an extra step forming between 610 °C and

 doi:10.20944/preprints202409.1957.v

650 °C. Also, in sample 6, the sharp and high exothermic DTA peak after 810 °C disappeared (did not form), so no new mineral formation occurred in this sample. The SEM images of the samples are given in Figure 7. Sample 2 contained Fe, Si, Al, Mg, O and C. Sample 5 contained Fe, Ca, Si, Mg and O, and sample 6 contained Fe, Si, Al, Mg and O. When we compare the samples to each other, the atomic percentages of both Mg and O are high compared to other elements. All the samples contained Fe, Si, Mg and O elements in their structures, but sample 2 contained C and sample 5 contained Ca. In addition, in sample 5, Al, which is present in the structure of the other samples, was not present. The X-ray diffraction patterns are shown in Figure 8. When the analysis results are evaluated, the types of serpentine minerals can be identified as lizardite, a small amount of chrysotile, and forsterite. The X-ray results support those of EDX analyses.

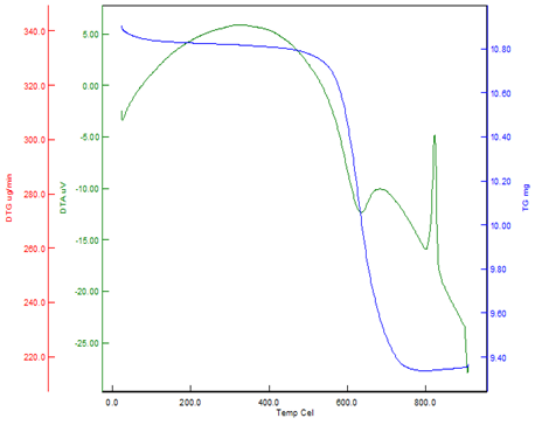

(**a**) Sample 2

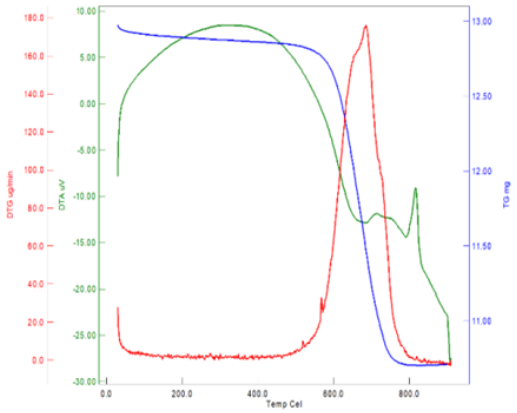

(**b**) Sample 5

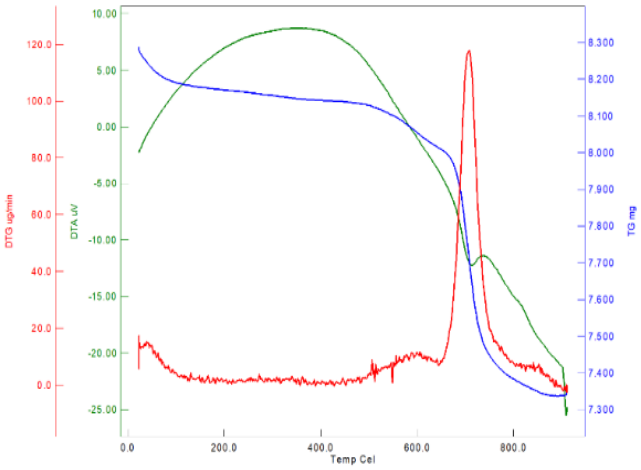

(**c**) Sample 6

Figure 6. The DTA and TGA thermograms of the serpentinite samples.

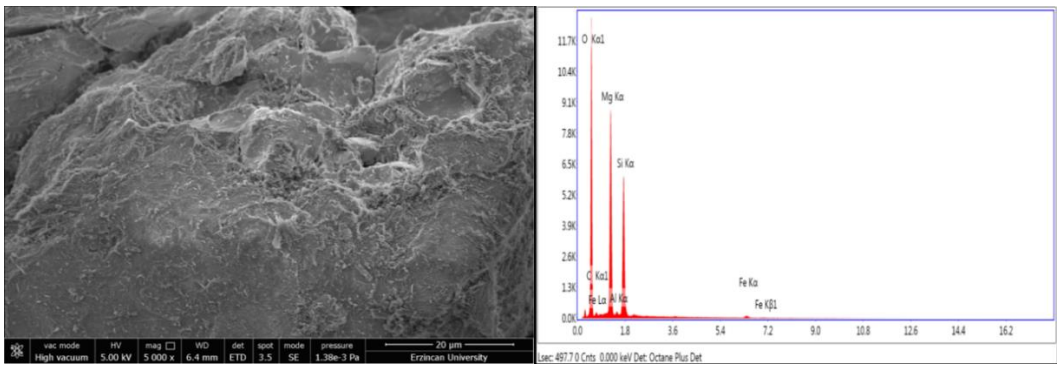

 doi:10.20944/preprints202409.1957.v

(a) Sample 2

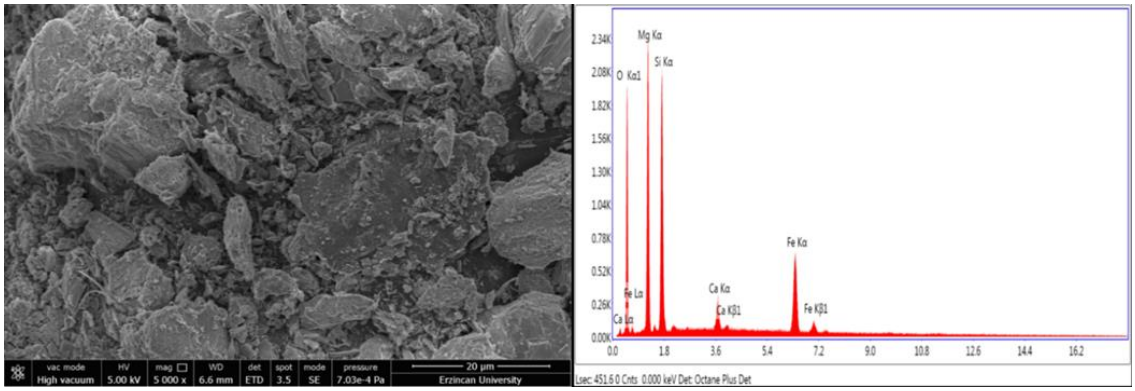

(b) Sample 5

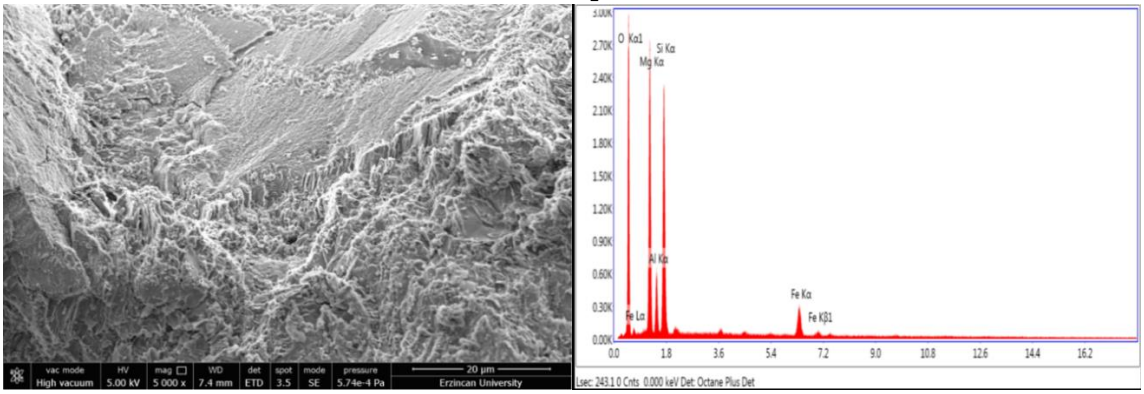

(c) Sample 6

Figure 7. SEM images of the serpentinite samples.

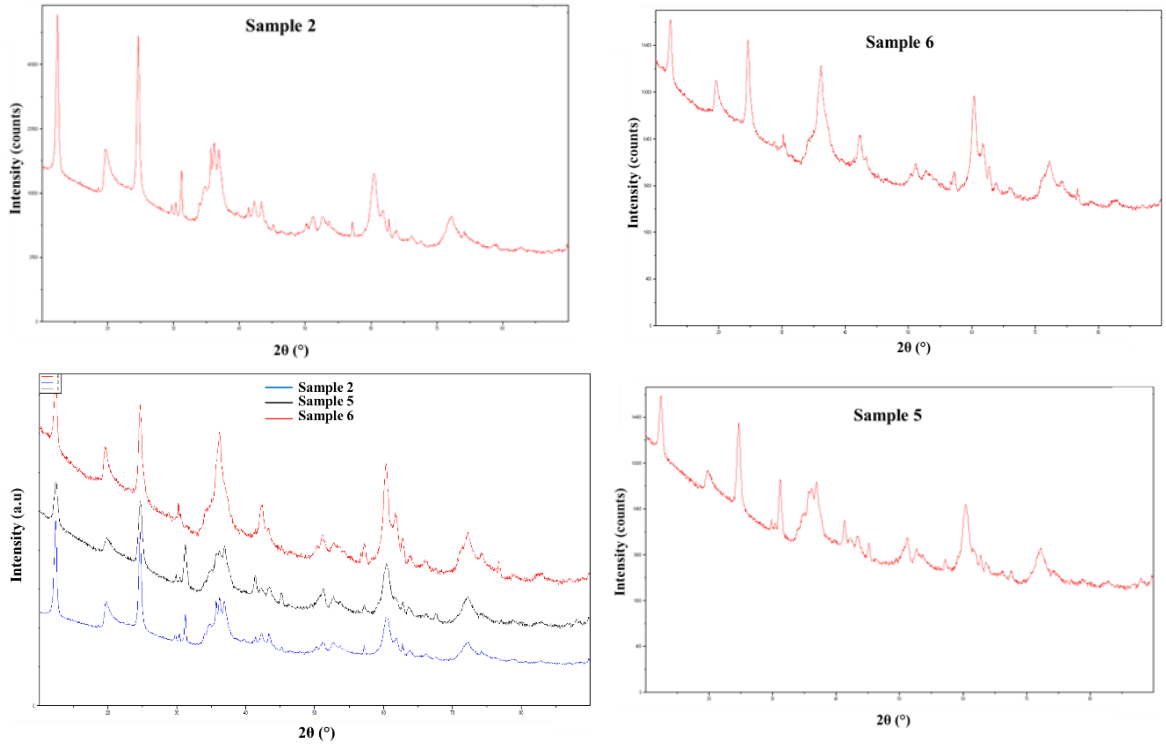

Figure 8. Whole-rock X-ray diffraction (XRD) spectra of selected samples.

5. Conclusions

 doi:10.20944/preprints202409.1957.v

The serpentinites exhibit highly intriguing physicochemical properties and possess sig-nificant potential for application in various industrial areas. However, despite this poten-tial, the number of studies conducted on these minerals remains relatively limited. Given the substantial reserves in Elazıg (Turkey), exploring new applications for serpentinites could give rise to important opportunities. Besides CO2 capture, utility in catalysis can al-so be considered, given this mineral group's strong adsorption capacity. Chrysotile is usually present in small and harmless amounts (<%5). It has seen use in industrial appli-cations throughout the 20th century. It shows such physical properties as flame resistance, high tensile strength, thermal insulation, and chemical resistance. It has been observed that lizardite and chrysotile, minerals derived from the serpentine group under study, are suitable for industrial use due to their high MgO and SiO2 contents.

The absence or scarcity of carbonate minerals (calcite, dolomite) in the serpentinites examined generally indicates that the XCO2 values given during serpentinization are negli-gibly low. In the MgO–SiO2–H2O–CO2 equilibrium system, the equilibrium temperatures required for the serpentinization reaction and the presence of chrysotile minerals (record-ed by SEM, TG and XRD analyses) are approximately 350-425 °C, depending on the pres-sure (Pf-PH2O). Guleman serpentinite samples are industrially durable serpentinites with high MgO (32-42 wt. %, except for Sp 01) and low Al2O3 contents (0.4-6.9 wt. %; Table 1). As a result, in the experimental studies of Johannes [11], serpentinization temperatures for chrysotile were found to be 350-425 oC, depending on the pressure. According to Barnes and O'Neil [19], lizardite and chrysotile are stable at temperatures below 350 °C. Moody [12] stated that the lizardite–chrysotile community is stable below 400–440 °C, and that antigorite develops at higher temperatures. So, serpentine minerals may feature areas of gradual stability depending on their composition (Fe and Al amounts), oxygen fugacity (Fe2+, Fe3+) and H2O activity [18]. Chrysotile and lizardite begin to form at temperatures <350 °C [19,40] and are stable at temperatures of 400-440 °C [19,46]. In mantle wedge ser-pentinites, this value indicates that serpentinization occurs at temperatures of 300-375 °C, and that liquids leaking from the plate are released at temperatures <200 °C (Alt and Shanks [40]). However, lizardite+talc+magnesite+chlorite paragenesis shows that this transition can develop at lower temperatures due to the influence of CO2-containing waters on serpentinites [49-51[. Above 460 °C, the serpentinite begins to produce olivine. Brucite is not detected at these temperatures. The theoretical place of this mineral in the transition from lizardite to antigorite is registered. Brucite, which is formed in low amounts, is con-sumed at high temperatures [52–56]. Therefore, this process may explain the lack of brucite observed in natural samples from subduction zones around the world.

Our study shows SEM images of the examined samples, showing that the serpentinite minerals are less chrysotile and predominantly lizardite. According to other analysis re-sults, a high MgO value indicates lizardite, while chrysotile developed along the cracks. The samples presented characteristics favorable to industrial raw materials when they were evaluated in terms of MgO content (36.67% on average) and SiO2 content (high at 35–43%). In a geological environment, Mg/Si varies between 1.18 and 1.38 (~1.33), the Mg# [Mg/(Mg+Fe)] values vary around 78–82, and the Ti value is > 100 ppm, indicating the presence of subduction zone serpentinites [30]. The ΣREE values in the analyzed serpen-tinites are 1–44, while the ΣLREE values are 0.8–6.22 and ΣHREE values are 0.6–38. The ΣLREE/ΣHREE ratios are 0.16-4. Additionally, the negative Ce anomaly (0.1–12) and the weakly positive Eu anomaly (0.1–0.3) are caused by the interaction between fluids and rock. Highly incompatible elements are an indication of fluid integration into the system during subduction [23]. In particular, elements such as U, K, Cs, and Rb are high in these serpentinites (~100 PM).

The large DTA peak in sample 2 at 810–830 °C is a sign of dehydration, transfor-mation reactions and thermal decomposition. Serpentine minerals, which are phyllosili-cates containing water in their crystal structure, begin to lose water around 800 °C. This occurs as an endothermic (heat sinking) peak in the DTA. Regarding the sample examined, the XRD data show that it is forsterite (Mg2SiO4). Additionally, at such high temperatures, olivine and pyroxene forsterite, enstatite and clinoenstatite may develop. A sudden de-crease in the mass of a sample around 800 °C under thermogravimetric analysis (TG or TGA) indicates the development of a significant mass loss in the TG curve as water mole-cules leave the structure during dehydration. Thermal decomposition at high temperatures can

 doi:10.20944/preprints202409.1957.v

cause a sudden decrease in mass. The decomposition products can often be gaseous or present in different solid phases, leading to mass loss. The presence of carbonate minerals (e.g., magnesite, $MgCO_3$) in the serpentinite sample also makes it possible that these car-bonates will thermally decompose at around 800 °C, releasing carbon dioxide (CO_2) gas. The sudden mass loss in the TG curve can be explained as forsterite transformation or CO_2 release. Similarly, the same situations apply in sample 5 and sample 6.

5. Conclusion

Residual mantle peridotites or ultramafic cumulates protoliths serpentinites is located in orogenic zones. These serpentinites consist of abyssal peridotites and mantle wedge peridotites; The protolith of Guleman serpentinites contains traces of primary orthopyroxene and olivine. These residual minerals indicate that the protoliths of the serpentinites were mantle peridotite dunite or harzburgite. Serpentine group minerals are formed by the hydration of silica-poor olivine/pyroxene minerals at relatively low temperatures [1,2].

Lizardite and a small amount of chrysotile species were found in the analyzed samples of the serpentine group, consisting of antigorite, chrysotile and lizardite. Guleman serpentinites contain varying amounts of lizardite and chrysotile. The absence of antigorite indicates that serpentinization occurs at low temperatures. Experimental studies of different researchers [9,11,13,24] have found serpentinization temperatures of 350–425 °C for chrysotile, 500 °C for antigorite, and 440 °C for lizardite+chrysotile.

SEM images of the examined samples and MgO-SiO_2, MgO-Fe_2O_3 and Ni-Ce diagrams also confirm the presence of chrysotile and lizardite minerals. In SEM images, the mineral with a planar structure is lizardite, while the mineral with a more spiral structure is chrysotile [9]. Guleman serpentinites are refractory serpentinites; high MgO (usually >35 wt%; Table 1), high Mg# (78-82), low Al_2O_3/SiO_2 (<0.01) and high MgO/SiO_2 (0.6-0.95) shows that it is high. Major element compositions show that the examined serpentinites are similar to the major element compositions of forearm/mantle wedge serpentinites and abyssal plate serpentinites, except for their refractory properties [69]. Because, Abyssal plate serpentinites exhibit higher FeO, lower SiO_2, MgO and Al_2O_3 contents compared to forearc/mantle wedge serpentinites.

The ΣREE values of the samples are between 1-44, the ΣLREE value is between 0.8-6.22, and the ΣHREE contents are between 0.6-38. The ΣLREE/ΣHREE ratios are 0.16-4 and high Ce (0.1-12) shows a weakly positive Eu anomaly (0.1-0.3). These features indicate fluid intrusion into the rock structure during serpentinization, during which Highly Incompatible Elements (HIEs) are gradually introduced into the serpentinization process. Additionally, as regards LREE enrichment, it was found that serpentinites do not undergo partial melting and structural changes with melt/rock interactions, and that the Pb content is high in serpentinites exhibiting this feature. All data show that the compositions of the examined samples are quite similar to the compositions of the mantle wedge/back rocks, but are contaminated by subduction components [6,70].

The large DTA peak in sample 2 at 810–830 °C is a sign of dehydration, transformation reactions and thermal decomposition. Serpentine minerals, which are phyllosilicates containing water in their crystal structure, begin to lose water around 800 °C. This manifests as an endothermic (heat sinking) peak under DTA.

The samples XRD data show that this was forsterite (Mg_2SiO_4). A peak at 810–830 °C on the DTA graph indicates dehydration or mineral phase transformations. At this temperature, serpentine, a hydrous phyllosilicate, is endothermic. The fact that serpentinites contain magnesite causes the release of CO_2 gas through thermal decomposition at approximately 800 °C, and the sudden mass loss in the TG curve indicates the release of forsterite and CO_2.

The refractory nature of the examined serpentine typically indicates that it is suitable for high-temperature applications, especially in industries requiring high temperatures such as metallurgy and steel production, the glass industry, ceramic manufacturing, and the chemical industry. Now, chrysotile is used in various industries such as sound, heat, and fire insulation, as well as in brake

 doi:10.20944/preprints202409.1957.v

linings, clutch pedals, and gasket materials. Chrysotile's remaining uses include in friction materials (7%), textiles, and other applications (10%) [57].

Funding: This study was supported by the Fırat University with FUBAP-MF 24.49 Project.

Data availability: Data can be provided upon request.

Conflicts of Interest: The authors declare no conflicts of interest.

References

1. Kılıç, A.D.; İnceöz, M. Mineralogical, geochemical and isotopic effect of silica in ultramaphic systems, eastern Anatolian Turkey. Geochemistry International 53, 369-382 (2015)
2. Dilek, Y.; Flower, M.F.J.; Arc-trench rollback and forearc accretion: 2. Model template for Albania, Cyprus, and Oman. In: Dilek, Y., Robinson, P.T. (Eds.), Ophiolites in Earth History, vol. 218. Geological Society of London, *2003*,43–68. Special Publication
3. Rakovan, J. Rocks Minerals **2011**, 98, 63
4. Evans, B.W.; Hattori, K.; Baronnet, A. Elements. **2013**, 9, 99
5. Wicks, F. J.; Whittaker E. J. W. A reappraisal of the structures of the serpentine minerals. *The Canadian Mineralogist* **1975**, 13 (3): 227–243
6. Evans, B.W. Lizardite versus antigorite serpentinite: magnetite, hydrogen, and life. *Geology* **2010**, 38, 879–882.
7. Morgan, A., Acid Leaching Studies of Chrysotile Asbestos from Mines In The Coalinga Region Of California And From Quebec And British Columbia. *Am. occup. Hyg*. **1997**, 41/3,249-268.
8. Klein, F.; Bach, W.; McCollom, T.M. Compositional controls on hydrogen generation during serpentinization of ultramafic rocks. *Lithos* **2013**, 178, 55–69.
9. O'Hanley, D. S.; Wicks, F. J. Conditions of formations of lizardite, chrysotile and antigorite, Cassiar, British Columbia, *Can. Mineral*. **1995**, 33, 753 – 773.
10. Sanna, A.; Wang, X.; Lacinska, A.; Styles, M.; Paulson, T.; Maroto-Valer, M. Enhancing Mg extraction from lizardite-rich serpentine for CO_2 mineral sequestration. *Minerals Engineering* **2013**, 49, 135-144.
11. Johannes, W. An experimental investigation of the system MgO-SiO2-H2O-CO2. *American Journal of Sci*ence **1969**, 267, 1083-1104.
12. Moody, J.B. Serpentinisation a review. *Lithos* **1976**, 9, 125-138.
13. Früh-Green, G.L.; Connolly, J.A.D.; Plas, A. Serpentinization of oceanic peridotites: Implications for geochemical cycles and biological activity. In: The Subseafloor Biosphere at Mid-Ocean Ridges, Geophys. *Am Geophys Union Monograph Se*r. **200**4, 144,119–136.
14. Page, N.J. Chemical differences among the serpentine Bpolymorphs. *Am Mineral* **1968**, 53,201–201.
15. Jones L. C.; Rosenbauer. R.; Goldsmith, J.I. Carbonate control of H2 and CH4 production in serpentinization systems at elevated P-T's. *Geophys Res Lett* **2010**, 37,1–6.
16. Andréani, M.; Baronnet, A.; Boullier, A.M.; Gratier, J.P. A microstructural study of a B crack-seal type serpentine vein using SEM and TEM techniques. *Eur J Mineral* **2004**, 16, 585–595.
17. Barnes, L.; Jr Le Marche,V.C.; Himmelberg,G.R. Geochemical evidence of present day serpentinization. *Science* 1967, 156, 830–832.
18. Sleep, N. H.; Bird, D.K,.; Pope, E. C. Serpentinite and the dawn of life. *Philos Trans Royal Soc London B* **201**1, 366, 2857–2869.
19. Barnes, I.;O'Neil, J.R. The relationship between fluids in some fresh Alpine-type ultramafics and possible modern serpentinization, Westem United States. Geol. Soc. Amer. Bull. **201**9, 80, 1947-1960.
20. Ulmer, P.;Trommsdorff, V. Serpentine Stability to Mantle Depths and Subduction-Related Magmatism, 1995, .268, 5212, 858-61.
21. Rouméjon, S.; Cannat, M. Serpentinization of mantle-derived peridotites at mid-ocean ridges: Mesh texture development in the context of tectonic exhumation. Geochem. *Geophys. Geosyst* **201**9, 15, 2354–2379.
22. Chittenden, E.T.; Stanton, D.J.; Watson, J.; Dodson, K.J. Serpentine and dunite as magnesium fertilisers. New Zealand. *J Agric Res* **1967**, 10(1): 160-171.
23. Mcnaught, K.J.; Dorofaeff, F.D.; Karlovsky, J. Effect of magnesium fertilisers and season on levels of inorganic nutrients in a pasture on Hamilton clay loam. New Zealand. *J Agric Re*s **1968**. 11, 3, 533-550.
24. Błońska, E.; Januszek, K.; Małek, S.; Wanıc, T. Effects of serpentinite fertilizer on the chemical properties and enzyme activity of young spruce soils. *Int Agrophys* **2016**, 30, 401-414.
25. Luz, A.B.; Loureıro, F.; Sampaıo, J.A.; Castılhos, Z.C.; Bezerra, M.S. Capítulo 4. Rochas, minerais e rotas tecnológicas para a produção de fertilizantes alternativos. In: Centro de Tecnologia *Mineral*s **2010**., 380.
26. Carmignano, O.; Vieira S.S. ; Paulo, B. ; Bertoli, A. ; Lago, R. M. Serpentinites: Mineral Structure, Properties and Technological Applications. *J. Braz. Chem. Soc*. **2019**, 00, 1-13.

27. Blaskowskı, A.E.; Bergmann, M.; Sılveıra, C.A.P.; Garnıer, J.; Camargo, M.A.; Cavalcante, O.A. Potencial das rochas das pilhas de rejeitos da mineração Ferbasa-Cia de Ferroligas da Bahia como corretivos e remineralizadores de solo. p. 121-127. In: Anais do III Congresso Brasileiro de Rochagem, 8 a 11 de novembro de 2016 / Adilson Luis Bamberg... et. al. (Eds). Pelotas: Embrapa Clima Temperado; Brasília: Embrapa Cerrados; Assis: *Triunfal Gráfica e Edit*ora **2016**, 455.
28. Moody, J.B. Serpentinization: Areview. *Lithos* 1976, 9(2), 25-138.
29. Hoskins, J.A. Chrysotile asbestos cement and the Grenfell Tower fire. Toxicol. Appl. *Pharmacol* **201**8, 361, 171. https://doi.org/10.1016/j.taap.2018.04.003
30. Nguyen, H.; Kaas, A.; Kinnunen, P.; Carvelli, V.; Monticelli, C.; Yliniemi, J.; Illikainen, M. Fiber reinforced alkali-activated stone wool composites fabricated by hot-pressing technique. *Mater.* Des. 2020, 186, 108-315. https://doi.org/10.1016/j.matdes.2019.108315.
31. Grozeva, N. G. Carbon and mineral transformations in seafloor serpentinization systems. PhD thesis, Massachusetts Institute of Technology, Cambridge, MA 2018.
32. Kakooei, H.; Marioryad, H. Evaluation of exposure to the airborne asbestos in an automobile brake and clutch manufacturing industry in Iran. *Regul. Toxicol. Pharmacol*. **2010**, 56 (2), 143–147. https://doi.org/10.1016/j.yrtph.2009.09.005.
33. Sakakibara, M.; Uehara, S. What is asbestos? *Rock Miner. Sci*. **2006**, 35, 3–10. https://doi.org/10.2465/gkk.35.3.
34. Znamenáčková, I.; Dolinská, S.; Lovás, M.; Hredzák, S.; Matik, M.; Tomčová, J.; Čablík, V. Application of microwave energy at treatment of asbestos cement (eternit). *IOP Conference Series: Earth and Environmental Science **2016***, 052023 https://doi.org/10.1088/1755-1315/44/5/052023.
35. Iwaszko, J. Making asbestos-cement products safe using heat treatment. *Case Stud. Constr. Mater.* **20**19, 10, e00221. https://doi.org/10.1016/j.cscm.2019.e00221.
36. Priest, G.; Horner, J.A. Fibrous ceramic aluminum silicate as an alternative to asbestos liners. *J. Prosthet. Dent.* **1980**, 44 (1), 51–56. https://doi.org/10.1016/0022-3913(80)90046-3.
37. Abrajano, T. A. Geochemistry of reduced gas related to serpentinization of the Zambales ophiolite, Philippines. *Appl. Geochem*istry **1990**, 5, 625–630.
38. McCollom, T. M. Geochemical constraints on primary productivity in submarine hydrothermal vent plumes. *Deep-Sea Res. Lett*er **2000**, 47, 85–101.
39. Carmingnano, O. Employment of serpentinite rock in architecture. *Journal of Material Science & Engineering* 2023, 301, 495–498.
40. Barne, I. ; O'Neil, J. R. The relationship between fluids in some fresh alpine-type ultramafics and possible modern serpentinization, western United States. *Geological Society of America Bullet*in 1969,80(10), 1947-1960.
41. Hostetler, P. B.; Coleman, R. G.; Mumpton, F.A.; Evans,B.W.Brucite in alpine serpentinites. *Am. Mineral*ogist **1966**, 51, 75 – 98.
42. Kilic, A.D.; Konakcı, N.; Sasmaz, A. Garnet Geochemistry of Pertek Skarns (Tunceli, Turkey) and U-Pb Age Findings. *Minerals*, **2024** 14,539.
43. Me´vel, C. Serpentinization of abyssal peridotites at mid-ocean ridges, *C.R. Geosci*. **2003**, 335, 825 – 852.
44. Cavallo, A. Resour. *Policy* **2018**, 59, 17.
45. Özkan, Y. Z. Guleman ofiyolitinde metamorfizma izleri, *TJK symposium (ın Turkish)* 1989, 11, 29-32.
46. Kılıç, A.D.; Yıldırım, Ö. Redox Reactions in Antigorite Serpentinites.3. *International Conference on Innovative Academic studies* **2023**, 26-28.
47. Deschamps, F.; Godard, M.; Guillot, S.; Hattori, K. Geochemistry of subduction zone serpentinites: A review. *Lithos* **2013**. 178, 96–127.
48. Yada, K.; Iishi, K.Serpentine minerals hydrothermally synthesized and their microstructures. *J. Crystal* Growth **1974**, 24/25, 627 – 630.
49. Niu, Y. Bulk-rock major and trace element compositions of abyssal peridotites: Implications for mantle melting, melt extraction and post-melting processes beneath mid-ocean ridges. *Journal of Petrology* 2004, 45, 2423–2458.
50. Ball, M.C.; Taylor, H.F.W. The dehydration of chrysotile in air and under hydrothermal conditions. *Mineral. Mag.* 1963, 33, 467–482.
51. Viti, C. Serpentine minerals discrimination by thermal analysis. *Am. Mineral*. **201**0, 95, 631–638.
52. Alt, J.C.; Shanks, W.C. Stable isotope compositions of serpentine seamounts in the Mariana forearc: Serpentinization processes, fluid sources and sulphur metasomatism. *Earth and Planetary Science Letters* **2006**, 242, 272–285.
53. McDonough, W.F. The composition of the Earth. *Chemical Geology* **1989**, 120, 3-4.
54. Surour, A.A. Chemistry of serpentine "polymorphs" in the Pan-African serpentinites from the Eastern Desert of Egypt, with an emphasis on the effect of superimposed thermal metamorphism. *Miner Petrol* **2017**, 111,99–119.
55. Renard, F.; Andreani, M.; Boullier, A.M.; Labaume, P.Crack-seal patterns: Records of uncorrelated stress release variations in crustal rocks, in Deformation Mechanisms, Rheology and Tectonics: From Minerals to the Lithosphere, edited by D. Gapais et al. *Geol. Soc. Spec. Publ.* **200**5, 243, 67 – 79.

 doi:10.20944/preprints202409.1957.v

56. Hattori, K.H.;Wallis, S.;Enami, T.; Mizukami,T. Subduction of mantle wedge peridotites: evidence from the Higashi-akaishi ultramafic body in the Sanbagawa metamorphic belt. *Island Arc* **201**0, 19, 192–207.
57. Hellebrand, E.; Snow, J.E.; Dick, H.J.B.; Hofmann,A.E. Coupled major and trace elements as indicators of the extent of melting in mid-ocean-ridge peridotites. *Nature* **200**1, 410, 677–681.
58. McDonough, W.F. The composition of the Earth. *Chemical Geology* 1989, 120, 3-4.
59. Niu, Y. Bulk-rock major and trace element compositions of abyssal peridotites: Implications for mantle melting, melt extraction and post-melting processes beneath mid-ocean ridges. *Journal of Petrology* **200**4, 45, 2423–2458.
60. Kelemen, P.B.; Hirth, G.; Shimizu, N.; Spiegelman, M., Dick, H.J.B. A review of melt migration processes in the adiabatically upwelling mantle beneath oceanic spreading ridges. *Philosophical Transactions of the Royal Society, London A* **199**7, 355, 283–318.
61. Wu , K.; Zhang, L.; Yuan, H.; Sun, W.; Deng, J.; Robert, E.; Zartman[b], E.; Guo , J.; Bao , Z.; Zong, J. Boron, arsenic and antimony recycling in subduction zones: New insights from interactions between forearc serpentinites and CO2-rich fluids at the slab-mantle interface. *Geochimica et Cosmochimica Acta* **2021**, *298, 21-42.*
62. Miyashiro, A.; Shido, F.; Ewing, M. Composition and origin of serpentinites from the Mid-Atlantic Ridge near 24 and 30°N. *Contributions to Mineralogy and Petrology* 1969, 23, 117–127.
63. MacLeod, C.J.; Escartín, J.; Banks, G. J.; Irving, D.H.B.; Lilly, R.M.; Niu, Y.L.; Banerji, D.; McCaig, A.; Allerton, S.; Smith, D.K. Direct geological evidence for oceanic detachment faulting: the Mid-Atlantic Ridge, 15°45′N. *Geology* **2002**, 30,879–882.
64. Davies, J. H.Simple analytic model for subduction zone thermal structure. *Geophysical Journal International* 1999, 139 (3), 823–828.
65. Kumar, A.;Cassetta, M.; Giarola, M.; Zanatta, M.; Le Guen, M.;Soraru, G.D.; Mariotto, G.Thermal Annealing and Phase Transformation of Serpentine-Like Garnierite. *Minerals* **202**1, 11(2), 188. https://doi.org/10.3390/min11020188
66. Abi, C. E.; Gürel S. B., Kılınç, D.; Emrullahoglu,Ö.F. Production of forsterite from serpentine–Effects of magnesium chloride hexahydrate addition. Advanced Powder Technology **2015**, 26(3), 947-953. https://doi.org/10.1016/j.apt.2015.03.011
67. Sun, Q;. Zhang, Y.;Dong, Z. Low-wave-velocity and high-electrical-conductivity layer of serpentine: a compilation. *Pure and Applied Geophysics* **2019**, 176, 4941-4954. https://doi.org/10.1007/s00024-019-02218-z
68. Fantini, R.; Sisti, M.; Arletti, R.; Malferrari, D.; Gamberini, M.C.; Zapparoli, M.; Gualtieri, A.F. Identification and quantification protocol of hazardous-metal bearing minerals: Ni in serpentinite rocks from Valmalenco (Sondrio, Central Alps, Northern Italy). *Journal of Hazardous Materials* **2024**, 134-928. https://doi.org/10.1016/j.jhazmat.2024.134928
69. Deschamps, F.; Godard, M; Guillot, S; HattoriK. Geochemistry of subduction zoneserpentinites: A review. ***Lithos*** **2013**, 178:96–127.
70. Savov, I.P.; Ryan, J.G.; D'Antonio, M.; Kelley, K.; Mattie, P. Geochemistry of serpentinizedperidotites from the Mariana ForearcConical Seamount, ODP Leg 125:İmplications for the elemental recycling atsubduction zones. *Geochemistry,Geophysics, Geosystems* **2005**a, 6,4.http://dx.doi.org/10.1029/2004GC00077